Hybrid Wave Propagation in Circularly Shielded Microslot Lines

Ioannis O. Vardiambasis, John L. Tsalamengas, and John G. Fikioris

Abstract—**Hybrid wave propagation in circularly shielded, single or coupled microslot lines is studied by combining singular integral equation (SIE) with Green's function techniques. Discretization of these SIE's by recently developed algorithms leads to linear algebraic systems whose matrix elements assume exponentially converging, numerically very stable analytical expressions. Dispersion characteristics, modal currents, and cutoff frequencies are presented for several cases. The algorithm converges rapidly requiring a few expansion functions per wavelength.**

I. Introduction

CIRCULARLY shielded microstrip-lines, slot-lines, and related structures are potentially useful in integrated-circuit technology for microwave and millimeter wave applications. They most advantageously exhibit a wide monomode bandwidth (useful, e.g., in building ultra-bandwidth microwave circuit elements such as hybrid junctions and directional and polarization-selective couplers), low dispersion, moderate attenuation, easy fabrication, and comformability with many microwave integrated-circuit-devices [1]–[5].

In comparison with corresponding rectangularly shielded lines their advantages [2] are two-fold: 1) they provide better control of field polarization (potentially useful in phase shifters, travelling-wave isolators, and antenna feeds); and 2) they possess better attenuation characteristics and thus they provide a potential alternative in the cases where, owing to increasing attenuation, rectangularly shielded lines become impractical.

In spite of their importance, which has long been recognized [1], dispersion characteristics of such structures have only recently received attention in [2] (based on the method of lines) and [3] (using the finite element method). As noted in [2] and [3] the main reason for this lack of attention was the complexity of the pertinent boundary value problems. It should be noted in this context that most of the analytical techniques applied to rectangularly shielded lines (e.g., the dual-series-equation method) are no longer applicable.

Using powerful direct singular integral equation techniques [6] an analytical study of the modes in circularly shielded striplines [7] and slot-lines [8] has most recently been reported. Both these structures support uncoupled TE and TM modes, which were investigated separately. In contrast, the microslot (and microstrip) configurations to be studied in this paper (Figs. 1 and 2) support hybrid waves. So, the propagation problem is now described by a system of coupled singular integral-integrodifferential equations (SIE-SIDE). These equations are constructed in Section II and discretized by the algorithms developed in [6] and [9]. Dispersion diagrams, current distribution of modes, and cutoff frequencies are presented in Section III.

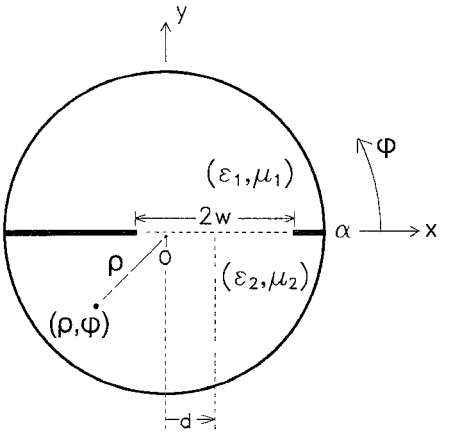

Fig. 1. Circularly shielded microslot.

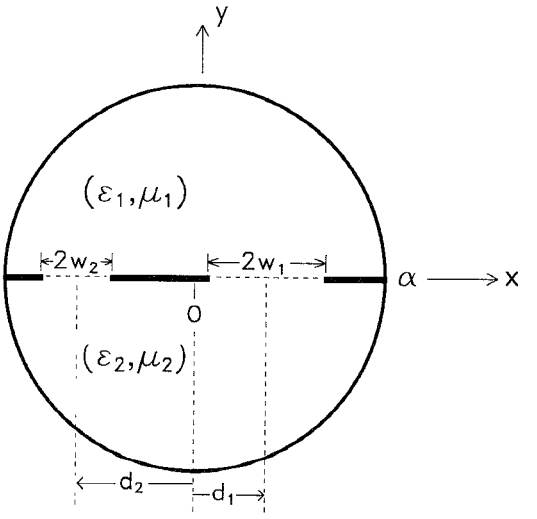

Fig. 2. Circularly shielded double microslot. The axes of the slots are at $x = d_1, x = -d_2$, respectively.

II. Formulation

Fig. 1 shows an off-centered, cylindrically shielded microslot of width $2w$ at $(y = 0, d-w \leq x \leq d+w, -\infty < z <$

Manucript received November 10, 1994; revised April 24, 1995.

The authors are with the Department of Electrical and Computer Engineering, National Technical University of Athens, GR-15773, Zografou, Athens, Greece.

IEEE Log Number 9412677.

∞) (d is the eccentricity). The radius of the cylindrical shield is denoted by α whereas the filling material is characterized by the scalar constants $(\varepsilon_1, \mu_1, k_1 = \omega\sqrt{\varepsilon_1\mu_1})$ (region 1, $0 < \varphi < \pi$), $(\varepsilon_2, \mu_2, k_2 = \omega\sqrt{\varepsilon_2\mu_2})$ (region 2, $\pi < \varphi < 2\pi$).

In contrast to the case $(\varepsilon_1 = \varepsilon_2, \mu_1 = \mu_2)$, wherein the guided waves are decomposed into TE and TM modes (which can be studied separately as outlined in [8]), the present configuration supports hybrid waves only. This more complicated propagation problem can be formulated in terms of a system of coupled SIE-SIDE, as outlined below. The $\exp(j\omega t)$ time-dependence, assumed for all field quantities, is suppressed throughout the following analysis.

A. Formulation of the System of SIE-SIDE

Let us define the equivalent surface magnetic current $\bar{M}(x) = \bar{E}(x,0) \times \hat{y} = M_z(x)\hat{z} + M_x(x)\hat{x}$. Invoking field equivalence principles the field $[\bar{E}^s(\bar{\rho}), \bar{H}^s(\bar{\rho})]e^{-j\beta z}$ at $\bar{\rho}(\rho, \varphi)$, see Fig. 1, inside region $s = 1$ (2) may be considered as the field produced by $\bar{M}(-\bar{M})$ in the absence of the slot (i.e., with the slot short-circuited).

We also introduce the fields $[{}^M\bar{E}^s(\bar{\rho}, \bar{\rho}'), {}^M\bar{H}^s(\bar{\rho}, \bar{\rho}')]e^{+j\beta z}$ and $[{}^J\bar{E}^s(\bar{\rho}, \bar{\rho}'), {}^J\bar{H}^s(\bar{\rho}, \bar{\rho}')]e^{+j\beta z}$ (phased-line-source Green's functions) which are excited at $\bar{\rho}(\rho, \varphi) \in (s)$ in the absence of the slot by the unit line-sources $(\bar{M}_a = \hat{z}M_a\delta(\bar{\rho} - \bar{\rho}')e^{j\beta z}(M_a = 1V)$ and $\bar{J}_a = \hat{z}I_a\delta(\bar{\rho} - \bar{\rho}')e^{j\beta z}(I_a = 1A)$, respectively, impressed at $\bar{\rho}'(\rho', \varphi') \in (s)\,(s = 1, 2)$. Clearly, ${}^JH_z^s = 0, {}^ME_z^s = 0$, since the two separate semicircular regions with homogeneous dielectrics do support TM respectively TE (to z) waves when excited by $\bar{J}_a$ respectively by $\bar{M}_a$.

Using the reaction theorem in the way outlined in [8] one gets the integral representations

$$M_aH_z^s(x', y') = \mathrm{sgn}(y')\int_C [M_x(x)\,{}^MH_x^s(x, 0; x', y') + M_z(x)\,{}^MH_z^s(x, 0; x', y')]\,dx \tag{1a}$$

$$-I_aE_z^s(x', y') = \mathrm{sgn}(y')\int_C M_x(x)\,{}^JH_x^s(x, 0; x', y')\,dx \tag{1b}$$

where C denotes the x-axis interval $d - w \le x \le d + w$. Here $jk_{cs}^2\,{}^MH_x^s(\bar{\rho}, \bar{\rho}') = -\beta\frac{\partial}{\partial x}{}^MH_z^s(\bar{\rho}, \bar{\rho}')$ and $jk_{cs}^2\,{}^JH_x^s(\bar{\rho}, \bar{\rho}') = -\omega\varepsilon_s\frac{\partial}{\partial y}{}^JE_z^s(\bar{\rho}, \bar{\rho}')$ where

$$\begin{pmatrix} {}^JE_z^s \\ {}^MH_z^s \end{pmatrix} = -\frac{k_{cs}^2}{4\omega}\begin{pmatrix} I_a\varepsilon_s^{-1}[H_0(k_{cs}R^-) - H_0(k_{cs}R^+)] \\ M_a\mu_s^{-1}[H_0(k_{cs}R^-) + H_0(k_{cs}R^+)] \end{pmatrix} + \sum_{n=0}^{\infty}\epsilon_nJ_n(k_{cs}\rho)J_n(k_{cs}\rho')\begin{pmatrix} B_n^s\sin(m\varphi)\sin(m\varphi') \\ A_n^s\cos(m\varphi)\cos(m\varphi') \end{pmatrix} \tag{2}$$

$$\epsilon_n = 2 - \delta_{n0} \quad \text{(Neumann's factor)},$$
$$R^{\pm} = \sqrt{(x - x')^2 + (y \pm y')^2}, \quad k_{cs}^2 = k_s^2 - \beta^2, \tag{3a}$$
$$A_n^s = M_a\frac{k_{cs}^2}{2\omega\mu_s}\frac{H_m'(k_{cs}\alpha)}{J_m'(k_{cs}\alpha)}, \quad B_n^s = I_a\frac{k_{cs}^2}{2\omega\varepsilon_s}\frac{H_m(k_{cs}\alpha)}{J_m(k_{cs}\alpha)}. \tag{3b}$$

(The Hankel function $H_m(\cdot)$ is of the second kind. $J_m(\cdot)$ denotes the Bessel function of order m). Note that z has been most naturally eliminated from (1a) and (1b) as a result of the $\exp(+j\beta z)$ dependence adopted for both $\bar{J}_a$ and $\bar{M}_a$ and the $\exp(-j\beta z)$ dependence for $\bar{E}^s$ and $\bar{H}^s$.

Letting $(y' = 0^{\pm}, x' \in C)$ in (1a) and using the boundary condition $H_z^{(1)}(x', 0^+) = H_z^{(2)}(x', 0^-)(x' \in C)$ we end up with the SIE

$$\mathcal{L}\{C; M_z, M_x; x'\} \equiv \sum_{s=1}^{2}\Bigg\{-k_{cs}^2L_s(M_z) + j\beta\frac{d}{dx'}L_s(M_x) + \sum_{n=0}^{\infty}\epsilon_nA_n^sJ_n(k_{cs}x')\Bigg[\int_C M_z(x)J_n(k_{cs}x)\,dx + \frac{j\beta}{2k_{cs}}\int_C M_x(x)h_n^-(k_{cs}x)\,dx\Bigg]\Bigg\} = 0, \ (x' \in C). \tag{4}$$

Here (and throughout the analysis that follows)

$$L_s(M) = L_s(M; x') = \frac{1}{2\omega\mu_s}\int_C M(x)H_0(k_{cs}|x - x'|)\,dx, \tag{5}$$

whereas $h_n^{\pm}$ are shorthand symbols for

$$h_n^{\pm}(k_cx) = J_{n-1}(k_cx) \pm J_{n+1}(k_cx). \tag{6}$$

The second, SIDE of the problem may be derived as follows: Substitute from (1a) and (1b) into $jk_{cs}^2H_x^s(x', y') = \beta\frac{\partial}{\partial x'}H_z^s(x', y') - \omega\varepsilon_s\frac{\partial}{\partial y'}E_z^s(x', y'); (x', y') \in (s)$; Set $(y' = 0^{\pm}, x' \in C)$ and apply the boundary condition $H_x^{(1)}(x', 0^+) = H_x^{(2)}(x', 0^-)$. Then, after some lengthy algebraic manipulations, one ends up with the SIDE

$$\mathcal{F}(C; M_z, M_x; x') \equiv \sum_{s=1}^{2}\Bigg\{j\beta\frac{d}{dx'}L_s(M_z) - \left[\frac{d^2}{dx'^2} + k_s^2\right]L_s(M_x) + \frac{1}{2k_{cs}}\sum_{n=0}^{\infty}\epsilon_n\Bigg[-j\beta A_n^sh_n^-(k_{cs}x') \times \int_C M_z(x)J_n(k_{cs}x)dx + \frac{1}{2k_{cs}}\int_C M_x(x)\big[\beta^2A_n^sh_n^-(k_{cs}x')h_n^-(k_{cs}x) + (\omega\varepsilon_s)^2B_n^sh_n^+(k_{cs}x')h_n^+(k_{cs}x)\big]\,dx\Bigg]\Bigg\} = 0 \quad (x' \in C). \tag{7}$$

B. Solution of the System of (4) and (7)

We change variables $x = d + wt, x' = d + wt'(-1 \le t, t' \le 1)$ and expand

$$M_z[x(t)] = (1 - t^2)^{-1/2}\sum_{N=0}^{\infty}a_NT_N(t),$$
$$M_x[x(t)] = (1 - t^2)^{1/2}\sum_{N=0}^{\infty}b_NU_N(t); \quad t = (x - d)/w \tag{8}$$

in conformity with the edge conditions (T_M and U_M are the Chebyshev polynomials). After inserting (8) into (4) and (7), multiplying both sides by $(1-t'^2)^{-1/2}T_M(t')$, respectively, $(1-t'^2)^{1/2}U_M(t')$, and integrating from $t'=-1$ to $t'=1$, we obtain the following linear algebraic system in a_N and b_N

$$\sum_{N=0}^{\infty}[a_N R_{MN}^{zz}+b_N R_{MN}^{zx}]=0,$$
$$\sum_{N=0}^{\infty}[a_N R_{MN}^{xz}+b_N R_{MN}^{xx}]=0;$$
$$M=0,1,2,\ldots \tag{9}$$

The matrix elements are given by

$$R_{MN}^{zz}=R_{MN}^{zz}(w,d)=w\sum_{s=1}^{2}\left[\frac{-k_{cs}^2}{2\omega\mu_s}A_{MN}(k_{cs}w)+\sum_{n=0}^{\infty}\epsilon_n A_n^s S_I^s(M,n)S_I^s(N,n)\right] \tag{10a}$$

$$R_{MN}^{xz}=R_{MN}^{xz}(w,d)=\frac{j\beta}{2}\sum_{s=1}^{2}\left[\frac{1}{\omega\mu_s}C_{MN}(k_{cs}w)-\frac{w}{k_{cs}}\sum_{n=0}^{\infty}\epsilon_n A_n^s\tilde{S}_-^s(M,n)S_I^s(N,n)\right] \tag{10b}$$

$$R_{MN}^{zx}=R_{MN}^{zx}(w,d)=-R_{NM}^{xz}(w,d), \tag{10c}$$

$$R_{MN}^{xx}=R_{MN}^{xx}(w,d)=\sum_{s=1}^{2}\left\{\frac{-1}{2\omega\mu_s w}D_{MN}(k_s^2,k_{cs}w)+\frac{w}{4k_{cs}^2}\sum_{n=0}^{\infty}\epsilon_n\times\left[\beta^2A_n^s\tilde{S}_-^s(M,n)\tilde{S}_-^s(N,n)+(\omega\varepsilon_s)^2B_n^s\tilde{S}_+^s(M,n)\tilde{S}_+^s(N,n)\right]\right\}. \tag{10d}$$

Here, 1) $A_{MN}(k_{cs}w), C_{MN}(k_{cs}w)$, and $D_{MN}(k_s^2,k_{cs}w)$—originating from the singular part of the kernels—assume the analytical, computationally very efficient expressions given in [9], and 2) S_P^s and $\tilde{S}_\pm^s$ are shorthand symbols for

$$S_P^s(M,n)=S_P^s(M,n;k_{cs}w,k_{cs}d)=\sum_{m=0}^{\infty}\frac{\epsilon_m}{2}[J_{n-m}(k_{cs}d)+(-1)^mJ_{n+m}(k_{cs}d)]\times P(M,m;k_{cs}w);P\equiv I,\Lambda, \tag{11a}$$

$$\tilde{S}_\pm^s(M,n)=\hat{S}_\pm^s(M,n;k_{cs}w,k_{cs}d)=S_\Lambda^s(M,n-1)\pm S_\Lambda^s(M,n+1) \tag{11b}$$

where

$$I(p,q;k_{cs}w)=\pi J_{(q+p)/2}(k_{cs}w/2)J_{(q-p)/2}(k_{cs}w/2),\quad \text{if } p+q \text{ is even, 0 otherwise} \tag{12a}$$

$$\Lambda(p,q;k_{cs}w)=[I(p,q)-I(p+2,q)]/2. \tag{12b}$$

One observes that when $d=0$ (symmetrically placed fins) $S_P^s(N,n)=P(N.n;k_{cs}w)$ $(P\equiv I,\Lambda)$. In this case, therefore, (10a)–(10d) involve single series solely which, as shown in [9], converge exponentially.

C. Two Radial Coplanar Microslots

For the cylindrically shielded structure of Fig. 2, encompassing two microslots at $C_1\equiv\{d_1-w_1\le x\le d_1+w_1;\ y=0\}$ and $C_2\equiv\{d_2-w_2\le x\le d_2+w_2;\ y=0\}$, the following relations:

$$\sum_{k=1}^{2}\mathcal{L}\{C_k;M_z^{(k)},M_x^{(k)};x'\}=0,$$
$$\sum_{k=1}^{2}\mathcal{F}\{C_k;M_z^{(k)},M_x^{(k)};x'\}=0\quad(x'\in C_1\cup C_2) \tag{13}$$

can be written with $\mathcal{L}$, $\mathcal{F}$ defined in (4) and (7). For convenience and without loss of generality, in what follows we will assume that $d_1>d_2$.

From (13) by setting successively $x'\in C_1$ and $x'\in C_2$ we get a 4×4 system of SIE-SIDE in the equivalent magnetic current densities $M_z^{(k)},M_x^{(k)}$ across the k-th slot $(k=1,2)$. From this system of SIE-SIDE, after expanding

$$M_z^{(k)}[x(t)]=(1-t^2)^{-1/2}\sum_{N=0}^{\infty}a_N^{(k)}T_N(t),$$
$$M_x^{(k)}[x(t)]=(1-t^2)^{-1/2}\sum_{N=0}^{\infty}b_N^{(k)}U_N(t);$$
$$t=(x-d_k)/w_k \tag{14}$$

we get, analogously to (9), the linear algebraic system

$$\sum_{N=0}^{\infty}\left\{\overline{\overline{R}}_{MN}^{(11)}\begin{bmatrix}a_N^{(1)}\\b_N^{(1)}\end{bmatrix}+w_2\,\overline{\overline{R}}_{MN}^{(12)}\begin{bmatrix}a_N^{(2)}\\b_N^{(2)}\end{bmatrix}\right\}=\begin{bmatrix}\bar{0}\\\bar{0}\end{bmatrix},$$
$$\sum_{N=0}^{\infty}\left\{w_1\,\overline{\overline{R}}_{MN}^{(21)}\begin{bmatrix}a_N^{(1)}\\b_N^{(1)}\end{bmatrix}+\overline{\overline{R}}_{MN}^{(22)}\begin{bmatrix}a_N^{(2)}\\b_N^{(2)}\end{bmatrix}\right\}=\begin{bmatrix}\bar{0}\\\bar{0}\end{bmatrix} \tag{15}$$

$(M=0,1,\ldots,\infty)$. For the elements of the 2×2 matrices $\overline{\overline{R}}_{MN}^{(ik)}=\begin{bmatrix}(R_{MN}^{zz})^{(ik)} & (R_{MN}^{zx})^{(ik)}\\(R_{MN}^{xz})^{(ik)} & (R_{MN}^{xx})^{(ik)}\end{bmatrix}(i=1,2;k=1,2)$ one ends up with the following analytical expressions: 1) For $i=k$

$$(R_{MN}^{uv})^{(i)}=R_{MN}^{uv}(w_i,d_i)\quad(u,v\equiv z,x;\ i=1,2) \tag{16a}$$

with $R_{MN}^{uv}(w_i,d_i)$ given in (10a)–(d), and 2) For $i\neq k$

$$(R_{MN}^{zz})^{(ik)}=\sum_{s=1}^{2}\left[2k_{cs}^2\Xi_{ik}^{II}(M,N;0)+\sum_{n=0}^{\infty}\epsilon_nA_n^s\hat{S}_I^i(M,n)\hat{S}_I^k(N,n)\right] \tag{16b}$$

$$(R_{MN}^{zx})^{(ik)}=j\beta\sum_{s=1}^{2}\left[-k_{cs}[\Xi_{ik}^{I\Lambda}(M,N;-1)-\Xi_{ik}^{I\Lambda}(M,N;1)]+\frac{1}{2k_{cs}}\sum_{n=0}^{\infty}\epsilon_nA_n^s\hat{\tilde{S}}_-^k(N,n)\hat{S}_I^i(M,n)\right] \tag{16c}$$

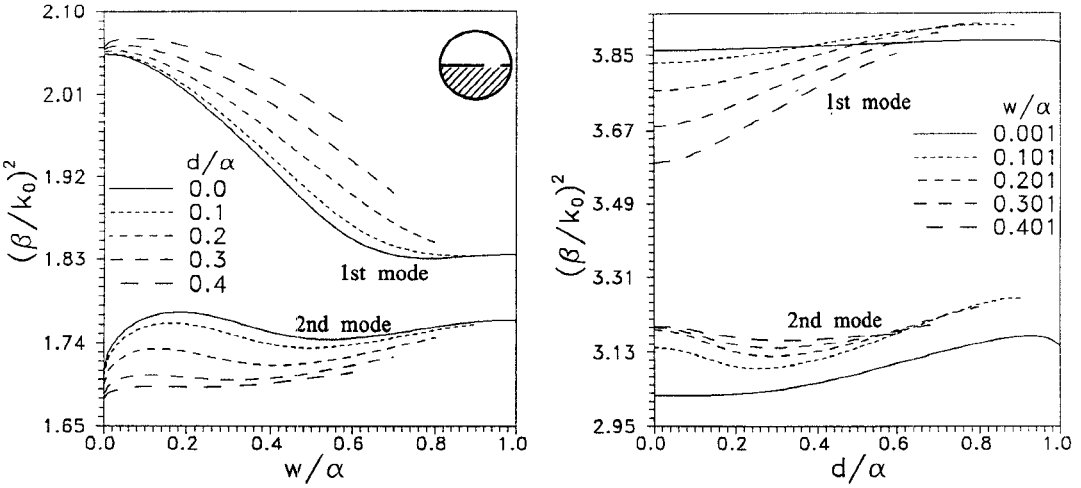

Fig. 3. (a) ε_{eff} versus w/α for several values of d/α (structure of Fig. 1, $\alpha/\lambda_0 = 0.567, \varepsilon_1 = \varepsilon_0, \varepsilon_2 = 2.32\varepsilon_0$). (b) ε_{eff} versus d/α for several values of w/α (structure of Fig. 1, $\alpha/\lambda_0 = 0.424, \varepsilon_1 = \varepsilon_0, \varepsilon_2 = 4.34\varepsilon_0$).

$$(R_{MN}^{xz})^{(ik)} = -j\beta \sum_{s=1}^{2} \left[k_{cs}[\Xi_{ik}^{\Lambda I}(M,N;-1) - \Xi_{ik}^{\Lambda I}(M,N;1)] + \frac{1}{2k_{cs}} \sum_{n=0}^{\infty} \epsilon_n A_n^s \hat{\tilde{S}}_-^i(M,n) \hat{S}_I^k(N,n) \right] \tag{16d}$$

$$(R_{MN}^{xx})^{(ik)} = \frac{1}{4} \sum_{s=1}^{2} \Big\{ [8k_s^2 \Xi_{ik}^{\Lambda\Lambda}(M,N;0) + 2k_{cs}^2 (\Xi_{ik}^{\Lambda\Lambda}(M,N;-2) + \Xi_{ik}^{\Lambda\Lambda}(M,N;2) - 2\Xi_{ik}^{\Lambda\Lambda}(M,N;0))] + \frac{1}{k_{cs}^2} \sum_{n=0}^{\infty} \epsilon_n (\beta^2 A_n^s \hat{\tilde{S}}_-^i(M,n) \hat{\tilde{S}}_-^k(N,n) + (\omega\varepsilon_s)^2 B_n^s \hat{\tilde{S}}_+^i(M,n) \hat{\tilde{S}}_+^k(N,n)) \Big\} \tag{16e}$$

where

$$\Xi_{ik}^{PQ}(M,N;\ell) = \frac{-1}{8\omega\mu_s} \sum_{n=0}^{\infty} \epsilon_n [\delta_{i1}(-1)^n + \delta_{i2}] \mathbf{H}_n(k_{cs}(d_1 - d_2)) \times \sum_{m=0}^{\infty} \epsilon_m [P(M,n+\ell+m;k_{cs}w_i) + (-1)^m P(M,n+\ell-m;k_{cs}w_i)] \times Q(N,m;k_{cs}w_k); \quad P,Q \equiv I,\Lambda \tag{17a}$$

$$\hat{S}_P^i(M,n) = S_P^s(M,n;k_{cs}w_i,k_{cs}d_i), \quad \hat{\tilde{S}}_\pm^i(M,n) = \tilde{S}_\pm^s(M,n;k_{cs}w_i,k_{cs}d_i). \tag{17b}$$

D. Special Case: Two Equal and Symmetrically Placed Coplanar Microslots

When $w_1 = w_2$ and $d_2 = -d_1$ (symmetrical case) one has either $\{M_z^{(1)}(x) = M_z^{(2)}(-x) \equiv M_z(x), M_x^{(1)}(x) = -M_x^{(2)}(-x) \equiv M_x(x)$; odd modes$\}$ or $\{M_z^{(1)}(x) = -M_z^{(2)}(-x) \equiv M_z(x), M_x^{(1)}(x) = M_x^{(2)}(-x) \equiv M_x(x)$; even modes$\}$. In this case (13) yield a 2×2 system of SIE-SIDE for the unknown densities M_z and M_x, defined just above and expanded as in (8), whose discretization leads to the linear algebraic system

$$\sum_{N=0}^{\infty} [a_N T_{MN}^{zz} + b_N T_{MN}^{zx}] = 0, \quad \sum_{N=0}^{\infty} [a_N T_{MN}^{xz} + b_N T_{MN}^{xx}] = 0; \quad M = 0,1,2,\ldots \tag{18}$$

Here

$$T_{MN}^{zz} = \tilde{R}_{MN}^{zz} \pm 2w(-1)^N \sum_{s=1}^{2} k_{cs}^2 \Xi_{12}^{II}(M,N;0) \tag{19a}$$

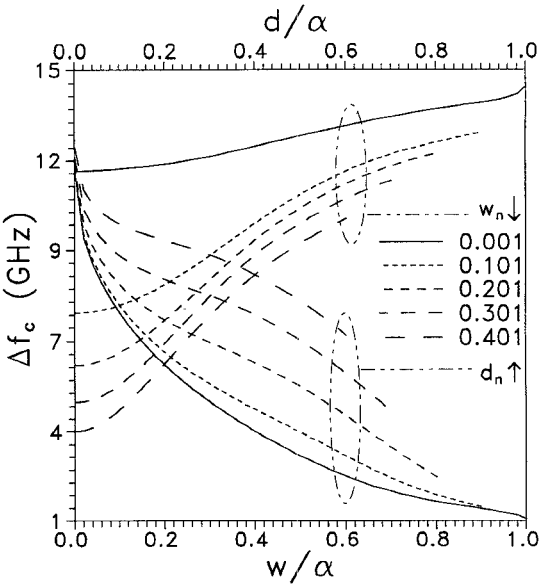

Fig. 4. Δf_c versus w/α for five values of $d_n = d/\alpha$; Δf_c vs d/α for five values of $w_n = w/\alpha$; (structure of Fig. 1, $\alpha = 3.175$ mm, $\varepsilon_1 = \varepsilon_0, \varepsilon_2 = 2.32\varepsilon_0$).

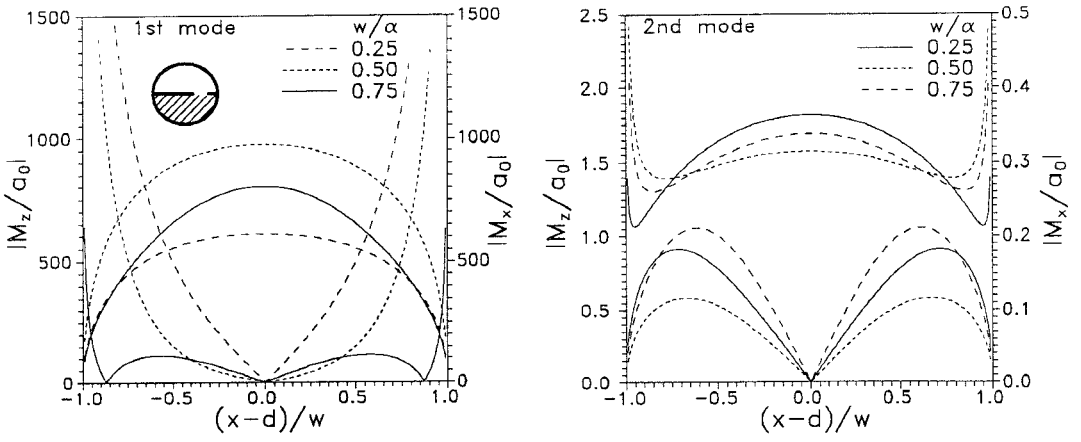

Fig. 5. $|M_z/a_0|$ and $|M_x/a_0|$ versus $(x-d)/w$ for three values of w/α (structure of Fig. 1, $\alpha/\lambda_0 = 1.0061, d = 0, \varepsilon_1 = \varepsilon_0, \varepsilon_2 = 2.32\varepsilon_0$). (a) 1st mode. (b) 2nd mode.

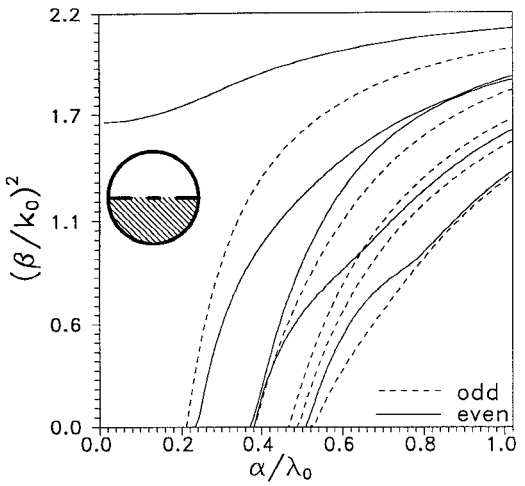

Fig. 6. ε_{eff} versus α/λ_0 for the first 10 modes (stucture of Fig. 2, $w_1 = w_2 = 0.3\alpha, d_1 = -d_2 = 0.5\alpha, \varepsilon_1 = \varepsilon_0, \varepsilon_2 = 2.22\varepsilon_0$).

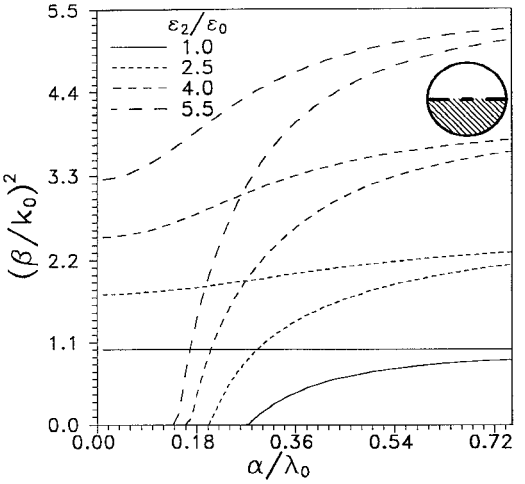

Fig. 7. ε_{eff} versus α/λ_0 for the first two modes and for several values of $\varepsilon_2/\varepsilon_0$ (structure of Fig. 2, $w_1 = w_2 = 0.3\alpha, d_1 = -d_2 = 0.4\alpha, \varepsilon_1 = \varepsilon_0$).

$$T^{zx}_{MN} = \tilde{R}^{zx}_{MN} \pm j\beta w(-1)^N \times \sum_{s=1}^{2} k_{cs}(\Xi^{I\Lambda}_{12}(M,N;-1) - \Xi^{I\Lambda}_{12}(M,N;1)) \quad (19b)$$

$$T^{xz}_{MN} = \tilde{R}^{xz}_{MN} \pm j\beta w(-1)^{N+1} \times \sum_{s=1}^{2} k_{cs}(\Xi^{\Lambda I}_{12}(M,N;-1) - \Xi^{\Lambda I}_{12}(M,N;1)) \quad (19c)$$

$$T^{xx}_{MN} = \tilde{R}^{xx}_{MN} \pm \frac{w}{4}(-1)^{N+1} \times \sum_{s=1}^{2}[8k_s^2\Xi^{\Lambda\Lambda}_{12}(M,N;0) + 2k_{cs}^2(\Xi^{\Lambda\Lambda}_{12}(M,N;-2) + \Xi^{\Lambda\Lambda}_{12}(M,N;2) - 2\Xi^{\Lambda\Lambda}_{12}(M,N;0))] \quad (19d)$$

with $\tilde{R}^{zz}_{MN}, \tilde{R}^{zx}_{MN}, \tilde{R}^{xz}_{MN}, \tilde{R}^{xx}_{MN}$ computed from (10a)–(d) after replacing A^s_n, B^s_n by $A^s_n(1 \pm (-1)^n), B^s_n(1 \pm (-1)^n)$ respectively; the upper (lower) sign corresponds to the odd (even) modes.

III. Numerical Results and Discussion

Figs. 3–5 pertain to the single-slot structure of Fig. 1.

Fig. 3(a) and (b) shows the effective dielectric constant $\varepsilon_{\text{eff}} = (\beta/k_0)^2$ as a function of w/α (of d/α) for several values of d/α (of w/α) for the first two modes. Clearly, the dispersion behavior of the structure is strongly influenced by changing d and/or w.

Fig. 4 shows the monomode bandwidth $\Delta f_c = f_{c2} - f_{c1}$ as a function 1) of w/α for several values of $d_n = d/a$ and 2) of d/α for several values of $w_n = w/a$, where $f_{c1}(f_{c2})$ is the cutoff frequency of the 1st (2nd) mode. Clearly, Δf_c can be controlled by suitably selecting the slot width and/or the eccentricity. As these plots reveal, an increase in d leads to an increase of Δf_c. (It is worth noting, also, that our results for the cutoff frequencies f_c turn out to be identical with those of [8] when $\varepsilon_1 = \varepsilon_2$, as expected. This is a partial check of the correctness of our algorithms.)

Fig. 5(a) and (b) shows the normalized modal currents $|M_z(t)/a_0|$ and $|M_x(t)/a_0|$ as a function of $t = (x-d)/w$ for

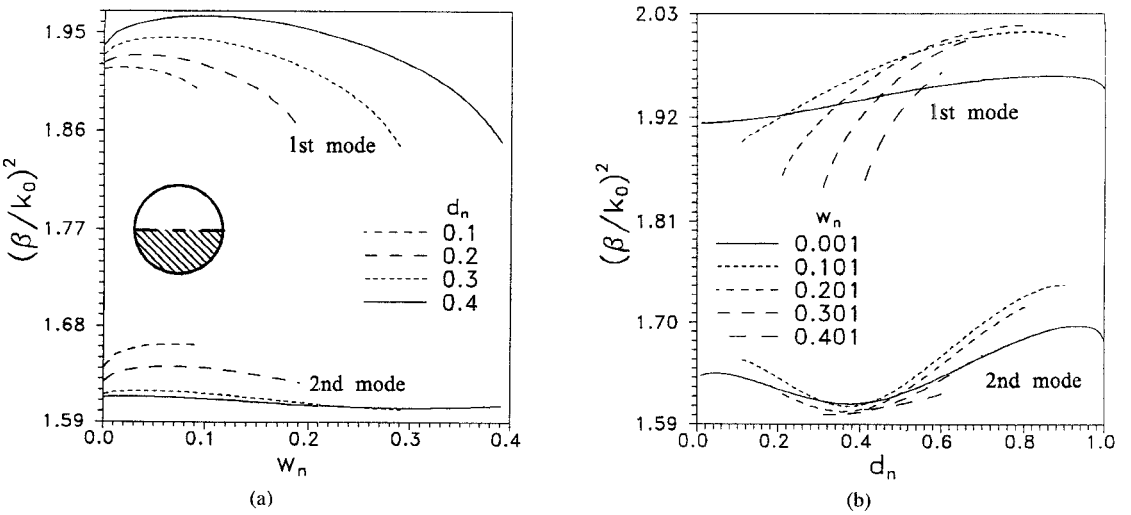

Fig. 8. (a) ε_{eff} versus w_n for four values of d_n (structure of Fig. 2, $\alpha/\lambda_0 = 0.5295, \varepsilon_1 = \varepsilon_0, \varepsilon_2 = 2.22\varepsilon_0$). (b) ε_{eff} versus d_n for five values of w_n (structure of Fig. 2, $\alpha/\lambda_0 = 0.5295, \varepsilon_1 = \varepsilon_0, \varepsilon_2 = 4.34\varepsilon_0$).

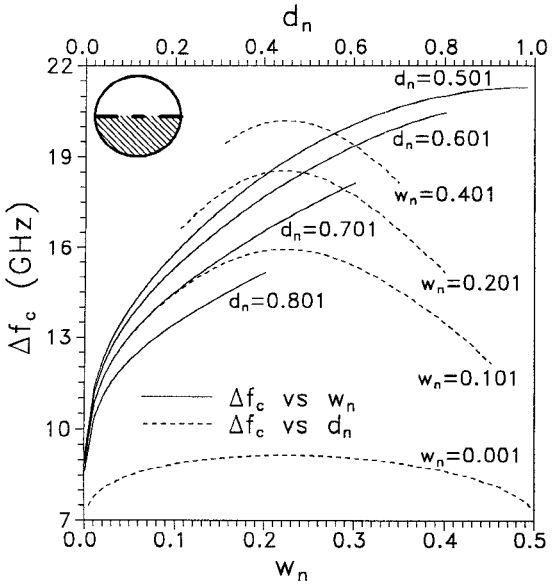

Fig. 9. Δf_c versus w_n for four values of d_n (solid curves); Δf_c versus d_n for four values of w_n (dashed curves) (structure of Fig. 2, $\alpha = 3.175$ mm, $\varepsilon_1 = \varepsilon_0, \varepsilon_2 = 2.22\varepsilon_0$).

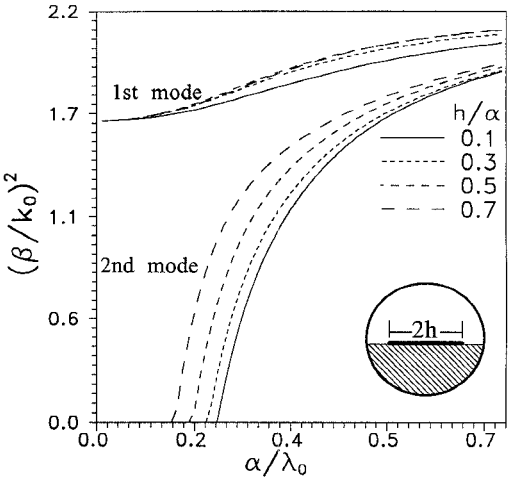

Fig. 10. ε_{eff} versus α/λ_0 for a circularly shielded symmetrical microstripline for the first two modes and for four values of $h/\alpha(\varepsilon_1 = \varepsilon_0, \varepsilon_2 = 2.22\varepsilon_0)$.

the 1st (2nd) mode. To achieve convergence, $N_r = 10$ basis functions were needed in each of (8).

Figs. 6–9 refer to a symmetrical double-slot configuration (Fig. 2: $w_1 = w_2, d_1 = -d_2$).

Fig. 6 shows ε_{eff} as a function of the normalized frequency α/λ_0 for the first 10 (even; solid lines, odd; dashed lines) modes when $w_1 = w_2 = 0.3\alpha, d_1 = -d_2 = 0.5\alpha, \varepsilon_1 = \varepsilon_0, \varepsilon_2 = 2.22\varepsilon_0$. As a check these curves were derived by (15) and, independently, by (18). Noticeable is the mode conversion phenomenon that occurs, e.g., between the 6th (even) and the 7th (odd) modes.

Analogous results for the first two modes and for several values of $\varepsilon_2/\varepsilon_0$ are shown in Fig. 7 when $w_1 = w_2 = 0.3\alpha, d_1 = -d_2 = 0.4\alpha, \varepsilon_1 = \varepsilon_0$.

Fig. 8(a) and ((b) shows ε_{eff} as a function of normalized width $w_n = w_1/\alpha = w_2/\alpha$ (of normalized eccentricity $d_n = d_1/\alpha = -d_2/\alpha$) for several values of d_n (of w_n) for the first two modes. Noticeable is once again the strong influence that may be exerted on the dispersion characteristics by changing d_n and/or w_n.

Fig. 9 shows the monomode bandwidth $\Delta f_c = f_{c2} - f_{c1} = f_{c2}$ as a function 1) of w_n for several values of d_n and 2) of d_n for several values of w_n. (In this case $f_{c1} = 0$, since the lowest order mode is TEM.) We observe that, for a given value of $d_n, \Delta f_c$ increases monotonically with increasing slot width w_n. In contrast, for a given value of $w_n, \Delta f_c$ attains a maximum value (occurring at moderate values of d_n).

The very practical configuration of a circularly shielded microstrip line (shown in the inset of Fig. 10) results from the structure of Fig. 2 in the limits $d_1 + w_1 \to \alpha; d_2 - w_2 \to -\alpha$. Its dispersion characteristics are shown in Fig. 10 in the symmetrical case, for the first two modes and for several strip widths (denoted by $2h$).

The convergence characteristics of the algorithm are illustrated in Table I, where ε_{eff} is shown for the 1st, 5th, and

TABLE I
CONVERGENCE OF THE ALGORITHM

	ε_{eff}		
N_r	1st mode	5th mode	10th mode
1	2.172203489	1.822293513	1.300070815
2	2.204315894	1.878139638	1.302310907
3	2.204448528	1.878327751	1.302902253
4	2.204227920	1.878043961	1.302369330
5	2.204227952	1.878043961	1.302370228
6	2.204227856	1.878043961	1.302369683
7	2.204227856	1.878043962	1.302369684

10th modes versus N_r, where N_r denotes the number of basis functions used in each of (8). These values correspond to the structure of Fig. 1 when $\alpha/\lambda_0 = 1.0061, w/\alpha = 0.25, d = 0, \varepsilon_1 = \varepsilon_0, \varepsilon_2 = 2.32\varepsilon_0$. Apparently the convergence is very rapid and stable. Thus, e.g., 2 basis functions suffice to determine ε_{eff} to within four significant decimals in all cases.

IV. CONCLUSION

Direct singular integral equation techniques have been effectively applied to solve for the propagation characteristics of hybrid waves in circularly shielded, single or coupled, microslot lines. The dependence of these characteristics on the geometrical parameters (such as eccentricity, slot-width, relative dielectric constant, radius of the shield) has been also investigated. The matrix elements are given by efficient analytical expressions and the algorithm is rapidly converging, requiring a few expansion functions. By following a limiting procedure, dispersion curves have been also presented for the practical structure of a circularly shielded microstrip line.

REFERENCES

[1] S. D. Robertson, "The ultra-bandwidth finline coupler," *Proc. IRE*, vol. 43, pp. 739–741, June 1955.

[2] K. Wu and R. Vahldieck, "The method of lines applied to planar transmission lines in circular and elliptical waveguides," *IEEE Trans. Microwave Theory Tech.*, vol. 37, no. 12, pp. 1958–1963, Dec. 1989.

[3] Eswarappa, G I Costache, and W. J. R. Hoefer, "Finlines in rectangular and circular waveguide housings including substrate mounting and bending effects—Finite element analysis," *IEEE Trans. Microwave Theory Tech.*, vol. 37, no. 2, pp. 266–306, Feb. 1989.

[4] A.-M. A. El-Sherbiny, "Cutoff wavelengths of ridged, circular, and elliptic guides," *IEEE Trans. Microwave Theory Tech.*, vol. MTT-21, pp. 7–12, Jan. 1973.

[5] H. N. Chait and N. G. Sakiotis, "Broad-band ferrite rotators using quadruply ridged circular waveguide," *IRE Trans. Microwave Theory Tech.*, vol. MTT-7, pp. 38–41, Jan. 1959.

[6] J. L Tsalamengas and J. G. Fikioris, "Efficient solutions for scattering from strips and slots in the presence of a dielectric half-space: Extension to wide scatterers: Part I—Theory; Part II—Applications," *J. Appl. Phys.*, vol. 70, no. 3, pp. 1121–1143, Aug. 1991.

[7] B. Babili, J. Tsalamengas, and J. Fikioris, "TM and TE modes in cylindrically shielded strip waveguides," *J. Electr. Waves Applications*, vol 6, no. 10, pp. 1291–1316, 1992.

[8] J. L. Tsalamengas, I. O. Vardiambasis, and J. G. Fikioris, "TE and TM modes in circularly shielded slot waveguides," *IEEE Trans. Microwave Theory Tech.*, vol. 41, no. 6/7, pp 966–973, June/July 1993.

[9] J. L. Tsalamengas, "Direct singular integral equation methods in scattering and propagation in strip or slot loaded structures," submitted for publication in *IEEE Trans. Antennas Propagat.*.

Ioannis O. Vardiambasis, photograph and biography not available at the time of publication.

John L. Tsalamengas, photograph and biography not available at the time of publication.

John G. Fikioris, photograph and biography not available at the time of publication.